Solvation–Reduction Coupling in Ca2+ Electroactivity in Glyme-Based Electrolytes: A First Principles Study

Long Hoang Bao Nguyen, Jean-sébastien Filhol

ADVANCED ENERGY MATERIALS
www.advenergymat.de

Solvation–Reduction Coupling in Ca^{2+} Electroactivity in Glyme-Based Electrolytes: A First Principles Study

*Long Hoang Bao Nguyen and Jean-Sébastien Filhol**

The electrochemical activity of solvated Ca^{2+} in glyme-based electrolytes is investigated using grand canonical density functional theory approach and Fukui functions. The obtained results reveal that the length of glyme molecules has little effect on the reduction potentials, but has significant impacts on the effective electron transfer process. In short chain glymes, the transferred electron is located on a Ca^{2+} center and the organic part of the solvation sphere, leading to a direct Ca^{2+} reduction and a partial degradation of the glyme molecules. As the glyme's length increases, the reduction process turns into the formation of solvated electrons rather than Ca^{2+} reduction, unless a partial desolvation occurs. Consequently, an effective Ca^{2+} reduction in long chain glyme-based electrolytes is controlled by a (partial) desolvation of the solvation sphere. These results can be used as guiding information to design new electrolytes having the Ca^{2+} reduction potential in an accessible voltage range together with an effective Ca^{2+} reduction process. The methodology developed in this study can be universally applied to investigate the thermodynamic and kinetic properties of other battery systems using metal anodes, which might lead to a paradigm shift in the design of prospective electrolytes for future battery technologies.

1. Introduction

Calcium-ion batteries (CIBs) have recently emerged as one of the future energy storage systems. Calcium, which is the fifth abundant element in the earth's crust, is ubiquitous and the use of CIBs will lead to an equal and sustainable development. CIBs are expected to provide a high operating voltage and capacity thanks to the low potential of the Ca^{2+}/Ca redox couple and the exchange of two electrons in electrochemical reactions.[1–5] The use of Ca metal anode can offer a gravimetric capacity of 1337 mAh g^{-1}, which outperforms Na metal anode (1165 mAh g^{-1}). Furthermore, a combination of two abundant elements, Ca and S, might result in Ca//S battery system which is expected to deliver an energy density of 1835 Wh kg^{-1}, compared to 2400 Wh kg^{-1} for Li//S.[6] Many signs of progress have recently been reported in this field, especially in the identification of suitable electrode materials which can allow a reversible insertion and extraction of Ca^{2+} in electrochemical reactions.[7–10] Nevertheless, the development of electrolytes for CIBs still lags behind with no optimal composition reported in the literature. Recent research focuses on using ether- or glyme-based electrolytes, due to their capability to dissolve a considerable amount of calcium salts, their high boiling point, and high stability over a wide electrochemical window.[11–16] The glyme family has the general chemical formula of $H_3CO(CH_2CH_2O)_nCH_3$, with the main representatives being dimethoxylethane or monoglyme (G1), diglyme (G2), triglyme (G3), or tetraglyme (G4) when n = 1, 2, 3, or 4, respectively. Recently, Zhao–Karger and Nazar groups have independently reported the possibility to perform a reversible Ca plating and stripping process using $Ca[B(HFIP)_4]_2$/G1 electrolytes ($[B(HFIP)_4]^-$ = tetrakis(hexafluoroisopropoxy) borate).[17–19]

Despites their low polarity and dielectric constant ($\epsilon_r \approx 7$), glymes can dissolve a considerable amount of salts thanks to their ability to form stable solvation complexes through strong M^{n+}–O bonds with the cation of interest. Depending on the chain length, glyme molecules can act as multidentate ligands and thus the solvated cation is greatly stabilized by the entropic contribution. Consequently, the solvated cation is more stabilized as the chain length increases. Nevertheless, a partial desolvation process is required to occur in the electrode's double layer for the calcium reduction and plating to take place during the battery operation, and thus such a strong solvation might lead to sluggish desolvation kinetics and a large overpotential. To ensure an equilibrium between ion dissociation and electrode kinetics, the reactivity of solvated ions in the double layer should be well apprehended. Furthermore, a detailed analysis of the reduction mechanism can help to rationalize whether the solvated ion is reduced

L. H. B. Nguyen, J.-S. Filhol
ICGM, Univ Montpellier, CNRS
ENSCM
Montpellier 34095, France
E-mail: jean-sebastien.filhol@umontpellier.fr
L. H. B. Nguyen, J.-S. Filhol
RS2E French Network on Electrochemical Energy Storage
Amiens FR5439, France

The ORCID identification number(s) for the author(s) of this article can be found under https://doi.org/10.1002/aenm.202300311

DOI: 10.1002/aenm.202300311

to the metal state or the whole solvation species will undergo a degradation with the formation of side products and a loss in the cyclability.

The thermodynamics and kinetics of Ca^{2+} reduction in the electrode's double layer can be achieved by employing potential dependent density functional theory (DFT) calculations developed by our research group.[20–22] In this approach, the solvated Ca^{2+} is placed at a distance of 8–10 Å from the Ca metal surface, representing the double-layer existing in all electrochemical systems. There is no direct orbital overlap at this distance, and the electron transfer between the two systems of interest can only occur through the tunneling effect. At this distance, the electron tunneling (typically 1 ps) would remain faster than the reorganization of the solvation sphere,[23] the Born–Oppenheimer approximation remains valid and the location of the reduction centers determined from the time independent DFT calculations should be reasonable. The potential where the Ca^{2+} reduction or decomposition reaction occurs can be determined by computing the variation in the free electrochemical energy of the Ca surface with and without the presence of the solvation species in the double layer, as discussed in ref. [20]. Furthermore, the redox centers participating in the electrode reactions can be identified using Fukui functions,[24,25] helping to determine whether Ca^{2+} or the organic chain is reduced in the electron transfer process.[20]

In this study, the electroactivity of solvated Ca^{2+} in G1 is first investigated within the framework of the potential dependent DFT calculations. The obtained results reveal that the fully solvated Ca^{2+} in G1 is susceptible to a direct Ca^{2+} reduction but associated to a partial decomposition of the solvation shell. When electrons are injected to the system, Ca plating occurs in parallel to the conversion of $[Ca(G1)_4]^{2+}$ to the non-electroactive species, $Ca(G1)_3(OCH_3)_2$. This behavior is similar to those reported for Mg^{2+} in our previous study.[21] In order to enable reversible Ca plating/stripping in G1 electrolytes, the utilization/addition of anions favoring the formation of ion-pairs is required. Bis(trifluoromethane)sulfonimide) or $TFSI^-$ is widely used due to its capability to form stable ion-pairs with Ca^{2+} in G1 solutions; however, these ion-pairs are unstable at low voltage and would decompose even before the Ca plating can occur. The concept is then extended to solvated Ca^{2+} in G4, a system exhibiting transitional properties between molecular and polymer solvents. A systematic comparison between G1 and G4 can provide an insightful information on the effects of chain length and solvent's multiplicity on the reactivity of solvated Ca^{2+}. The obtained results reveal important information on electrode reaction mechanism in long chain glyme-based electrolytes: i) the electroactivity of G4 is different from G1 even if they exhibit similar binding energy to Ca^{2+}, ii) the formation of solvated electrons rather than calcium reduction would be observed when Ca^{2+} attains its maximum coordination number of eight, and iii) the reduction of Ca^{2+} together with a weakening of Ca–O bonds can only occur efficiently when Ca^{2+} is partially de-coordinated, for example, to a coordination of five or six. These observations can be used as guiding information in the design of novel electrolytes for rechargeable CIBs.

2. Calculational Details

The solvation structures of Ca^{2+} in G1 and G4 reported in refs. [17, 18, 26] are used as input models for the potential dependent DFT calculations. In G1 solvent, Ca^{2+} is coordinated by four G1 molecules to achieve a coordination number of eight as discussed in the work of Zhao–Karger and Nazar groups.[17,18] On the other hand, Ca^{2+} in G4 exhibits a diverse solvation structure with the coordination number varying between five and eight, as discussed in recent studies.[26,27] In order to perform potential dependent DFT calculations that mimic the interfacial interaction between the solvated ions and Ca surface, a symmetric unit cell is created, and the molecular solvated structures are placed at a distance of 8–10 Å from the Ca surface to avoid all the direct interactions between the two systems. Ca (100) surface is used in this study. DFT calculations are performed using the Vienna ab initio simulation package (VASP)[28,29] within the framework of the Perdew–Burke–Ernzerhof[30] exchange-correlation functional with the Grimme DFT-D3[31] correction to include van der Waals interactions in the system. The influence of outer solvent molecules on the first solvation sphere is taken into account using the polarizable continuum model (PCM) provided in VASPSOL.[32,33] The PCM is parameterized with the solvent dielectric constant, which is $\epsilon_r = 7.20$ and 7.50 for G1 and G4, respectively. All calculations are performed with a cut-off energy of 550 eV and a k-points grid of $3 \times 3 \times 1$. Structural relaxation is performed on all atoms except the central Ca layer of the slab, and the residual forces after structural relaxation are lower than 0.02 eV $Å^{-1}$. The cavitation energy is set to zero in all calculations and the cavity size is defined by a cut-off electron density of 5×10^{-5}. Molecular geometries and Fukui functions are visualized with VESTA or Materials Studio.[34]

The surface potential in a vacuum scale (E_{vacuum}) is extracted directly from calculations performed with VASPSOL and converted to the standard hydrogen electrode (SHE) scale by using $E_{SHE} = E_{vacuum} - 4.50$ or Ca^{2+}/Ca scale by using $E_{Ca} = E_{vacuum} - 1.63$. The interface electrochemical effects are investigated through the surface charging and the interface free electrochemical energy (F) is calculated in the grand canonical ensemble formalism as discussed in our previous works.[20–22,35,36] For each interface system, a free electrochemical energy (F) computed at different applied potentials has a typical parabola shape. The electrochemical potential of a redox pair is determined from the crossing points of the parabolas associated with the corresponding interfaces. A detailed description of the equations used to develop the methodology for interfacial energy calculations and Fukui functions is given in Sections S1 and S2, Supporting Information.

3. Results

3.1. Electrochemical Activity of Solvated Ca^{2+} in G1

The symmetric unit cell presenting the interfacial interaction between solvated $[Ca(G1)_4]^{2+}$ ion and Ca (100) surface is de-

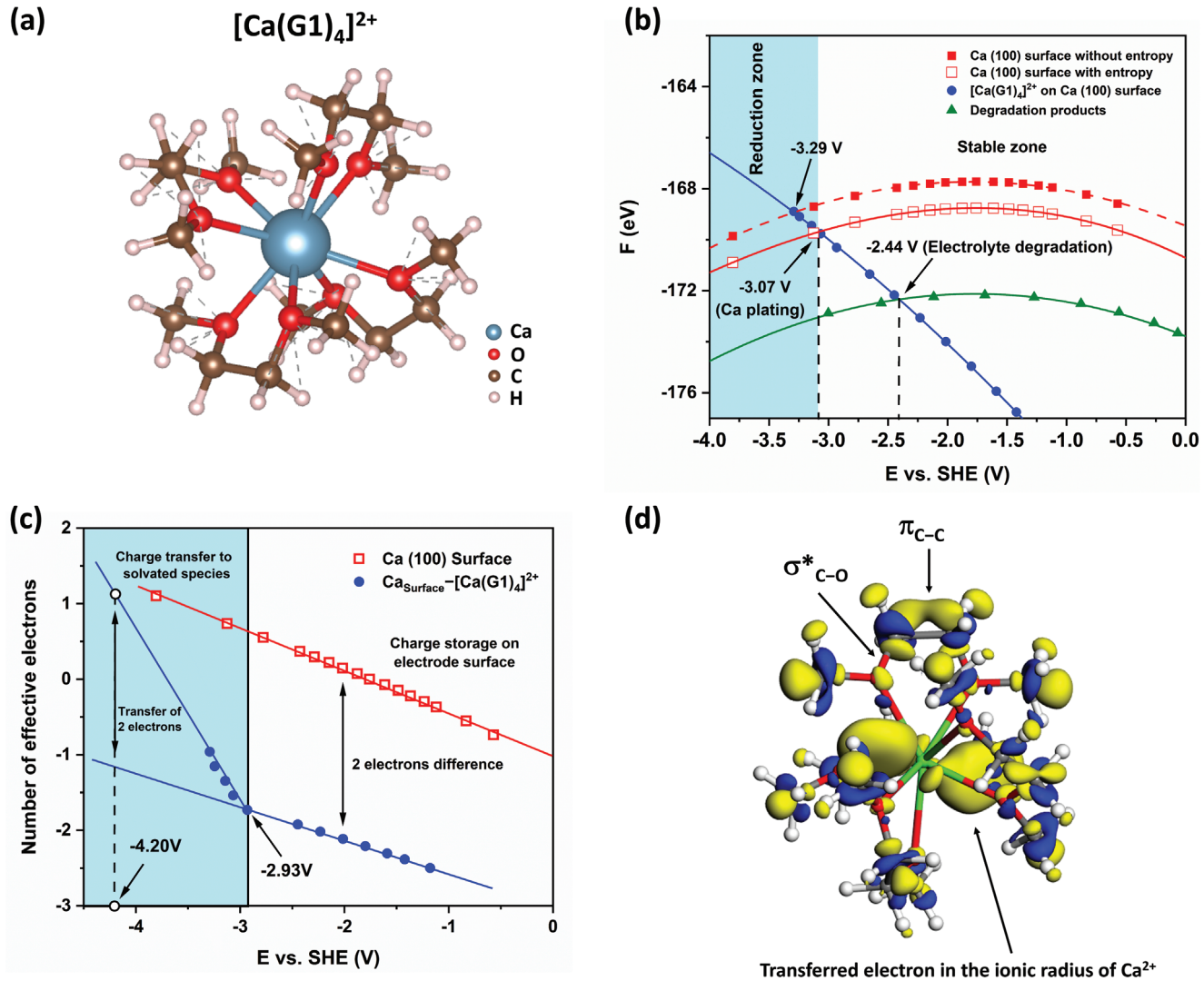

Figure 1. a) Solvation structure of Ca^{2+} in G1 electrolytes. Each Ca^{2+} possesses a coordination number of eight with four G1 molecules in its first solvation sphere. b) Free electrochemical energy (F) computed for the reduced (red) and oxidized (blue) Ca interfaces involved in the electrochemical reactions occurring at the electrode–electrolyte interface in the G1-based electrolytes. According to the methodology, the potentials at which free electrochemical energies of the two interfaces cross corresponds to the equilibrium potential of the considered reactions. The energy of Ca (100) surface without and with the entropy contribution from the release of G1 molecules are depicted as filled and open red squares, respectively. The energy of the degradation products, $Ca(G1)_3(OCH_3)_2$ and C_2H_4, is represented by green triangles. Thermodynamically, the $[Ca(G1)_4]^{2+}$ solvation species would be converted to the electro-inactive $Ca(G1)_3(OCH_3)_2$ below −2.44 V_{SHE}, even before the reduction of Ca^{2+} can occur. c) Evolution in the number of effective electrons added to the unit cell of two systems: Ca (100) surface and $Ca_{surface}$–$[Ca(G1)_4]^{2+}$. d) Fukui function calculated for $[Ca(G1)_4]^{2+}$ at −3.29 V_{SHE}. The yellow and blue areas indicate electron accumulation and depletion, respectively.

picted in Figure S1, Supporting Information. The electron transfer process can occur between Ca surface and solvated $[Ca(G1)_4]^{2+}$ (**Figure 1**a), existing in the electrochemical double layer, leading to the expected interface electrochemical Reaction (1).

$$\left\{Ca_{surface} - \left[Ca(G1)_4\right]^{2+}\right\} + 2e^- \leftrightarrows Ca_{surface} + Ca_{bulk} + 4G1 \quad (1)$$

The potential where Reaction (1) occurs can be predicted by comparing the free electrochemical energy of Ca surface with and without the presence of $[Ca(G1)_4]^{2+}$ in the double layer. The evolution in the energy of the two systems as the function of the applied potential is given in Figure 1b. The crossing of the oxidized and reduced surfaces gives a potential of −3.29 V versus SHE (i.e., −0.42 V vs $Ca^{2+}{}_{(aq)}/Ca$). According to Reaction (1), four G1 molecules confined in the first solvation shell are released into the electrolyte when the reduction occurs, and thus entropic contributions should be considered. Assuming the entropy associated to the release of G1 is similar as in the phase transition reaction $G1_{(solid)} \rightarrow G1_{(liquid)}$, the entropic term can be estimated from the fusion enthalpy and melting temperature of G1.[37] By taking into account the entropic contribution, a potential of −3.07 V_{SHE} (i.e., −0.20 V vs $Ca^{2+}{}_{(aq)}/Ca$) is obtained (Figure 1b). This value is associated with the thermodynamic stability of the redox pair,

and an equilibrium in the electron transfer between the electrode and the solvation species would occur at this potential. Another approach to probe the electron transfer between Ca surface and solvation species is following the evolution in the number of effective electrons added to simulated cells at different potentials ($N_{eff} = f(E)$). For a bare Ca(100) surface without the presence of $[Ca(G1)_4]^{2+}$, all the injected electrons will be accumulated on the top layer of the Ca surface as in the case of a capacitor, leading to a linear evolution in the number of effective electrons at different potentials (Figure 1c). When a neutral $[Ca(G1)_4]$ cluster is placed above the Ca surface, the structural and electronic optimizations lead to a spontaneous ionization of two electrons from the cluster to Ca surface together with the formation of $[Ca(G1)_4]^{2+}$ and a negatively charged surface. The $N_{eff} = f(E)$ curve of $\{Ca_{surface}\text{-}[Ca(G1)_4]^{2+}\}$ is shifted by about two electrons when compared to that of Ca surface (Figure 1c). When the potential decreases, extra electrons are injected to the system, in which two physical entities can accept electrons, that are, a negatively charged Ca surface and $[Ca(G1)_4]^{2+}$. For $E > -2.93$ V_{SHE}, the $N_{eff} = f(E)$ relation of $\{Ca_{surface}\text{-}[Ca(G1)_4]^{2+}\}$ system runs parallel to that of Ca(100) surface, indicating that all the injected electrons are confined on the top layer of Ca electrode. However, a rupture in the $N_{eff} = f(E)$ relation is observed at $E < -2.93$ V_{SHE} (Figure 1c), implying a change in electron storage mechanism, which is an electron capture process by $[Ca(G1)_4]^{2+}$. At the equilibrium potential (-3.07 V_{SHE}), the difference in the number of electron between Ca(100) and $Ca_{surface}\text{-}[Ca(G1)_4]^{2+}$ systems is 2.2, in which two electrons participate in the reduction process while 0.2 electron is required for the surface polarization. Reaction (1) is thus re-written as:

$$\left\{Ca_{surface} - \left[Ca(G1)_4\right]^{2+}\right\} + 2.2e^- \leftrightarrows Ca_{surface} + Ca_{bulk} + 4\,G1 + 0.2e^- \quad (2)$$

The charge transfer process is also confirmed by a change in the integrated charge surrounding the $[Ca(G1)_4]^{2+}$ cluster (Figure S2, Supporting Information). For $E > -2.93$ V_{SHE}, the $[Ca(G1)_4]$ cluster bears a constant charge of +2; however, the electron transfer between Ca surface and $[Ca(G1)_4]^{2+}$ starts to occur at $E < -2.93$ V_{SHE} together with a diminution in the charge of the solvated cluster. As the $[Ca(G1)_4]^{2+}$ cluster bears a charge of +2, the transfer of two electrons is required to completely neutralize the charge on the cluster. An extrapolation of the $N_{eff} = f(E)$ curve for $\{Ca_{surface}\text{-}[Ca(G1)_4]^{2+}\}$ system indicates that a complete charge neutralization with the transfer of two electrons would occur at -4.20 V_{SHE} (Figure 1c).

The potential dependent DFT calculations provide three different potential values corresponding to different phenomena:

a) Equilibrium thermodynamic reduction potential for Ca plating, which is the intercept in the $F = f(E)$ function of Ca surface and $\{Ca_{surface}\text{-}[Ca(G1)_4]^{2+}\}$ system (Figure 1b).
b) Onset potential of the electron transfer between Ca surface and $[Ca(G1)_4]^{2+}$ cluster, which is the rupture in the $N_{eff} = f(E)$ curve for $\{Ca_{surface}\text{-}[Ca(G1)_4]^{2+}\}$ (Figure 1c).
c) Extrapolated neutralized potential, at which the charge on the cluster vanishes completely (Figure 1c). This potential corresponds to the end of the reduction process and is an estimation of the maximum overpotential for the Ca plating process.

The potential range required for Ca^{2+} reduction in G1, predicted by DFT calculations, agrees with the experimental observations reported by Nazar group, in which the Ca plating from a 0.5 M $Ca[B(HFIP)_4]_2$/G1 solution took place at -0.55 V versus Ca^{2+}/Ca, that is, -3.42 V_{SHE}.[18]

All the calculated potentials only provide information on the thermodynamics of the reduction of $[Ca(G1)_4]^{2+}$ on Ca surface, without any implication on the effective electron transfer between them. Note that a reduction process occurs when the electron is transferred from the electrode surface to the solvated species; nonetheless, the transferred electron can locate on the Ca^{2+} center, the organic part, or the exterior of the solvation sphere. An effective reduction process can only occur when the transferred electron is located on the Ca^{2+} center. The information on the redox centers which may imply an effective reduction process can be accessed using Fukui functions. The Fukui analysis at -3.29 V_{SHE} reveals that the electron transferred from the electrode surface is distributed in the ionic radius of the Ca^{2+} center and on the organic part of the solvation sphere, indicating that there is a competition between Ca^{2+} reduction and the decomposition of the coordinating ligands (Figure 1d). In the organic part of the solvation sphere, the electron is distributed mainly on the orbital having the π_{C-} and σ^*_{C-O} character (Figure 1d), implying that the G1 molecule would decompose into methoxides/methanolates (CH_3O^-) and ethylene (C_2H_4). Therefore, the Ca plating process would occur in parallel with the decomposition of the organic molecule in the solvation sphere. As the Fukui function predicts the possible decomposition of the solvation shell during the reduction process, a new simulation cell mimicking the $\{Ca_{surface}\text{-}[Ca(OCH_3)_2(G1)_3] + C_2H_4\}$ system was generated and the evolution in the free electrochemical energy of this system is given in Figure 1b (Green curve). The obtained results show that $[Ca(G1)_4]^{2+}$ would thermodynamically convert to $Ca(OCH_3)_2(G1)_3$ at $E < -2.44$ V_{SHE} and the decomposition product, $Ca(OCH_3)_2(G1)_3$, is not electroactive. Even though thermodynamics predicts that $[Ca(G1)_4]^{2+}$ would decompose to $Ca(OCH_3)_2(G1)_3$ before the reduction reaction can occur, a kinetic hindrance could exist and prevent the conversion of $[Ca(G1)_4]^{2+}$ to $Ca(OCH_3)_2(G1)_3$. This observation is supported by the fact that the structural optimization does not lead to a spontaneous departure of C_2H_4 from the solvation sphere in the studied potential range. In reality, Ca plating can be achieved from Ca^{2+}/G1 solution as reported by several research group;[17–19] however, the reversibility will fade after each cycle due to the gradual formation of $Ca(OCH_3)_2(G1)_3$ in the competitive side reaction.

Similar decomposition has also been reported for Mg^{2+} system. In G1 solution, Mg^{2+} is preferentially solvated in the $[Mg(G1)_3]^{2+}$ form; nonetheless, Mg^{2+} is highly electrophilic and solvated $[Mg(G1)_3]^{2+}$ ions are metastable species under reduction conditions. When the electrode potential falls below -2.90 V_{SHE}, the structure became unstable and the structural optimization of $[Mg(G1)_3]^{2+}$ on Mg (0001) surface led to a spontaneous departure of ethylene from the solvation shell together with the formation of $Mg(OCH_3)_2(G1)_2$.[21] Furthermore, the Fukui analysis indicated that the transferred electron was located only on the organic part of the solvation sphere[21] and not on the Mg center suggesting that G1 decomposition would be more efficient than Mg^{2+} reduction. This phenomenon would degrade the electrolyte

gradually, leading to a loss in the performance of the cell in latter cycles. In the case of $[Ca(G1)_4]^{2+}$, the structural optimization does not result in this spontaneous fragmentation, but the Fukui function still implies a competitive reduction of Ca^{2+} and its solvation shell (Figure 1d). The difference in the electroactivity of Mg^{2+} and Ca^{2+} could be due to the fact that Mg^{2+} is a harder Lewis acid than Ca^{2+}[38–40] and the organic part coordinating to Mg^{2+} is more polarized, making it more electrophilic and thus more prone to reduction.

The work of Nazar group pointed out a gradual loss in the Ca plating and stripping capability of the $Ca[B(HFIP)_4]_2$/G1 solution,[18] where we can now attribute to the conversion of $[Ca(G1)_4]^{2+}$ to the non-electroactive species, $Ca(OCH_3)_2(G1)_3$. The same authors also reported that a stable cyclability could be achieved by employing a small amount of $[N(Bu)_4]Cl$, and this improvement was explained by an increase in the solution ionic conductivity and the diffusion coefficient of solvated Ca^{2+}.[18,41] From the thermodynamic point of view, an increase in the solution conductivity or Ca^{2+} diffusion coefficient cannot suppress the $[Ca(G1)_4]^{2+} + 2e^- \rightarrow Ca(OCH_3)_2(G1)_3 + C_2H_4$ reaction. Recent research in the field of Mg-ion batteries also reveals that Mg plating and stripping can be achieved in glyme-based electrolytes; however, their cyclability is relatively low without the use of Cl-containing additives.[42–45] Our group has recently demystified these observations and showed that Mg^{2+} has a strong electrophilicity which tends to decompose some of the organic molecules in its first coordination sphere, the degradation products, that is, $Mg(OCH_3)_2(G1)_2$, are non-electroactive, leading to a loss in the cyclability.[21] Cl^- has a great affinity to Mg^{2+} and when added to the electrolyte, it can compete with solvent molecules, leading to the formation of new solvation species, including $MgCl_2(G1)_2$, $[Mg_2Cl_2(G1)_4]^{2+}$, and $[MgCl_3(G1)]^-$.[22] The electron transfer from Cl^- ligands to Mg^{2+} reduces the electrophilicity of Mg^{2+} sites, preventing the degradation of the solvated ions. Furthermore, these Cl-containing species are electroactive, which ensures a long-term Mg plating and stripping process.[21,22] By analogy to Mg system, we can speculate that when $[N(Bu)_4]Cl$ is added into $Ca[B(HFIP)_4]_2$/G1 solution, Cl^- could participate into the coordination to Ca^{2+}, reducing its electrophilicity, preventing the formation of degradation products and enhancing the cyclability. Similar effect has also been reported for $Ca(BH_4)_2$/glyme electrolytes, in which BH_4^- was speculated to participate in the first solvation sphere of Ca^{2+} and favor reversible Ca plating/stripping processes.[46]

Care should be taken when choosing anions to stabilize contacting ion-pairs in electrolytes for CIBs. When $Ca[B(HFIP)_4]_2$ or $Ca(BH_4)_2$ in G1 is replaced by $Ca(TFSI)_2$, Ca^{2+} exists primarily in the form of contacting ion-pair $[Ca(G1)_3(TFSI)]^+$, but no reversible Ca plating/stripping can be achieved from $Ca(TFSI)_2$/G1 solutions.[11,13–15] In order to obtain insightful information on the reaction mechanism of this system, potential-dependent calculations were performed on the $Ca_{surface}$-$[Ca(G1)_3(TFSI)]^+$ system with the $[Ca(G1)_3(TFSI)]^+$ structure was pre-optimized at the same level of theory. During the structural optimization step on Ca metal, the $TFSI^-$ is fragmented spontaneously into and $F_3CSO_2NSO_2^-$ and CF_3^- without any charge transfer on Ca^{2+} center at $E < -2.9$ V_{SHE}. This structural fragmentation is even more pronounced when more electrons are injected to the system, where the CF_3^- is detached completely from the initial $TFSI^-$ and drifts away from the rest of the structure (Figure S4, Supporting Information). This structural decomposition occurs even before the thermodynamic reduction of Ca^{2+} to Ca^0 could occur. The reduction instability of $TFSI^-$ in $[Ca(G1)_3(TFSI)]^+$ contacting ion-pair is assigned to the polarization effect induced by the direct contact with Ca^{2+}. This observation agrees with experimental results showing that $TFSI^-$ would decompose into $F_3CSO_2NSO_2^-$ and CF_3^- in reduction conditions.[47] Therefore, the choice of salts and solvents has a great impact on the electroactivity of solvated Ca^{2+} in solutions.

3.2. Electrochemical Activity of Solvated Ca^{2+} in G4

In order to understand the impact of the length of glyme molecules on the electrochemical reactivity of solvated Ca^{2+}, potential dependent DFT calculations are also performed on G4-based electrolytes. In G4 solution, Ca^{2+} exhibits a great flexibility in its solvation structure depending on the amount of G4.[26] In diluted solutions, Ca^{2+} adopts the *mer*-$[Ca(G4)_2]^{2+}$ solvation structure where it is coordinated by eight oxygens [4 + 4] coming from two G4 chains (**Figure 2**a), which is thereafter referred as η^8-$[Ca(G4)_2]^{2+}$. The number following the η symbol indicates the number of oxygen atoms coordinating directly to the Ca^{2+} in the first solvation sphere. In G4-deficit conditions, Ca^{2+} is solvated by one G4 chain to obtain a coordination number of five in the form $[Ca(G4)]^{2+}$ (Figure 2d), referred as η^5-$[Ca(G4)]^{2+}$. An intermediate structure between these two, possessing two G4 molecules with six Ca–O bonds [5 + 1] in the first solvation shell, denoted as η^6-$[Ca(G4)_2]^{2+}$, is also considered. This latter form represents the partial desolvation structure of η^8-$[Ca(G4)_2]^{2+}$ that might exist in the double layer at the electrode surface. The difference in the number of Ca–O bonds in different solvation forms might result in a difference in their electroactivity, which is an interesting subject for discussion. The simulation cells of the two extreme cases, η^5-$[Ca(G4)]^{2+}$ and η^8-$[Ca(G4)_2]^{2+}$, are given in Figures S5 and S6, Supporting Information.

Figure 3a shows that the thermodynamic potential for η^8-$[Ca(G4)_2]^{2+}$ reduction on a Ca electrode surface would occur at -3.06 V_{SHE}. This value shows little difference as in $[Ca(G1)_4]^{2+}$ due to the similar Ca–O interaction energy in the two cases (-182.9 compared to -181.6 kJ mol^{-1} per Ca–O bond as in G4 and G1, respectively). On the other hand, the partially desolvated species, η^6-$[Ca(G4)_2]^{2+}$ and η^5-$[Ca(G4)]^{2+}$, exhibit the respective reduction potentials at -2.43 and -1.78 V_{SHE} (Figure 3a), which are more accessible than that of $[Ca(G1)_4]^{2+}$ or η^8-$[Ca(G4)_2]^{2+}$. This observation is consistent with the fact that by reducing the number of Ca–O bonds in the solvation shell, the solvated species become less stable and is prone to reduction. Nonetheless, the energy difference between η^5-$[Ca(G4)]^{2+}$/η^6-$[Ca(G4)_2]^{2+}$ and η^8-$[Ca(G4)_2]^{2+}$ is so large that the low coordinated Ca^{2+} can only present at a negligible population at a high potential, which cannot impact the thermodynamic potential for Ca^{2+} reduction.

Beyond the thermodynamics, an idea on the kinetics of electroreduction is given by the $N_{eff} = f(E)$ (Figure 3b), as seen above for G1. The onset potential values reveal that the facility of the electron transfer process depends strongly on the coordination number of the solvated Ca^{2+}, at which the electron transfer would occur easier for the form with less Ca–O bonds. **Figure 4**a shows

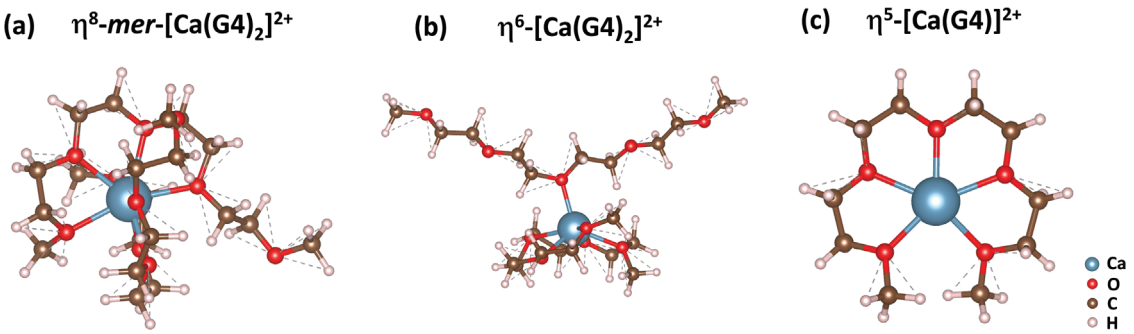

Figure 2. Different solvation structures of Ca^{2+} in G4 used in the interface calculations. The coordination number of the Ca^{2+} center is indicated by the number following the hapticity index (η).

the Fukui function for η^8-$[Ca(G4)_2]^{2+}$ system at −3.35 V_{SHE}. The Fukui function shows an obvious electron accumulation in the second solvation sphere, indicating that the electron transferred from the Ca surface is not accepted within the solvation shell of the $[Ca(G4)_2]^{2+}$ complex, but staying in the proximity of the solvated Ca^{2+} as a solvated electron (e_s^-). The existence of "cation–e_s^-" ion pairs in glyme solutions has been reported in the literature and the strength of the interaction in the ion pair depends on the temperature and the chelating ability of the glymes.[48,49] This reaction mechanism is completely different from $[Ca(G1)_4]^{2+}$ where a competitive reduction is expected to occur between the Ca^{2+} center and the organic part of the first solvation shell. In the case of η^8-$[Ca(G4)_2]^{2+}$, the formation of "η^8-$[Ca(G4)_2]^{2+}$–e_s^-" ion pair leads to an inefficient direct reduction of the Ca^{2+} center and thus induces sluggish kinetics for the Ca plating process.

As the direct reduction pathway being impractical, an alternative approach for an effective Ca^{2+} reduction would be the partial desolvation of η^8-$[Ca(G4)_2]^{2+}$. In order to study the impact of the partial desolvation on the electroactivity of Ca^{2+} in G4, the energy and effective charge transfer as a function of potential ($F = f(E)$ and $N_{eff} = f(E)$), and Fukui functions for the intermediate structure, η^6-$[Ca(G4)_2]^{2+}$, are calculated (Figures 3 and 4b). At $E < -2.26$ V_{SHE}, the $N_{eff} = f(E)$ curve for η^6-$[Ca(G4)_2]^{2+}$ increases gradually (blue curve in Figure 3b), which is similar to that of η^8-$[Ca(G4)_2]^{2+}$. The integrated charge on the η^6-$[Ca(G4)_2]$ cluster indicates an effective electron transfer from Ca surface to this solvation species (Figure S7, Supporting Information). Nonetheless, the associated Fukui function shows the presence of the electron in the exterior of the solvation sphere (Figure 4b), indicating the presence of a solvated electron without any effective reduction on the Ca^{2+} center. When the potential goes below −2.92 V_{SHE} (black open square in Figure 3a), the solvation sphere undergoes a structural reorganization into a new electroactive species characterized by an elongation of Ca–O bonds by 0.1 Å (Figure S8, Supporting Information). The simulation cells containing the structure of non-electroactive and electroactive η^6-$[Ca(G4)_2]$ are given in the Crystallographic Information Files in the Supporting Information. The Fukui analysis of this new form reveals that the added electron is located within the ionic radius of the Ca^{2+} center. Furthermore, the presence of this electron induces a polarization on the underlying 3p orbitals of Ca^{2+} (Figure 4c), indicating a direct reduction of Ca^{2+} to Ca^0. Furthermore, the Ca–O distance in this electroactive form elongates rapidly as the potential goes down (Figure S8, Supporting Information), indicating a weaker interaction between the ligand and the Ca^{2+} center, implying a partial formation of reduced Ca. This new electroactive η^6-$[Ca(G4)]^{2+}$ form possesses different energy and structural behavior than the initial η^6-$[Ca(G4)]^{2+}$. As shown in Figure 3a, the non-active η^6-$[Ca(G4)]^{2+}$ is more stable at $E > -2.92$ V_{SHE} while it would convert to the electroactive form when the potential goes below this limit. The presence of the electroactive η^6-$[Ca(G4)]^{2+}$ is more dominant as the potential goes lower. Interestingly, the free energy curve of the electroactive η^6-$[Ca(G4)]^{2+}$ becomes more stable than η^8-$[Ca(G4)_2]^{2+}$ at −3.68 V_{SHE}, inducing the desolvation of η^8-$[Ca(G4)_2]^{2+}$ and thus the Ca plating process, but at the cost of a large overpotential.

The observation in $[Ca(G4)_2]^{2+}$ system suggests that a partial desolvation of Ca^{2+} is required to obtain the calcium reduction and plating process. To test this hypothesis, the evolution in the free electrochemical energy of η^5-$[Ca(G4)]^{2+}$ at different potentials is calculated (yellow curve in Figure 3a). The result reveals that the electron transfer to this solvation species would occur at −1.48 V_{SHE}. Furthermore, the Fukui function associated with this species at −1.92 V_{SHE} clearly shows a pure reduction center located on Ca^{2+} (Figure S9, Supporting Information) together with an increase in the Ca–O distances, meaning that Ca^{2+} in η^5-$[Ca(G4)]^{2+}$ could be efficiently reduced without the formation of solvated electrons nor degradation of the organic part in the solvation sphere. Unfortunately, the free energy curve of η^5-$[Ca(G4)]^{2+}$ is higher than that of η^8-$[Ca(G4)]^{2+}$ or η^6-$[Ca(G4)]^{2+}$ (active form), and thus η^5-$[Ca(G4)]^{2+}$ can hardly be formed in solution.

4. Discussions

In recent studies, Schmickler group has proposed that the cation reduction mechanism depends strongly on the solvent and the nature of the cation participating in the electrode reactions.[50] For some cations such as Zn^{2+}, the reduction reaction can occur while the cation is in the fully solvated state.[51,52] On the other hand, a partial desolvation and an adsorption on the electrode surface is required for the reduction to occur, as for Fe^{2+}.[51] Nevertheless, the proposed concept was derived from a rigorous theoretical approach by considering the simplified electrode–electrolyte interface and the surface electron transfer process. In this study, the reduction mechanism of solvated Ca^{2+} in glyme-based electrolytes is visualized through an atomic representation, including electron interaction between electrode and solvated species, as calculated in the framework of the first principles

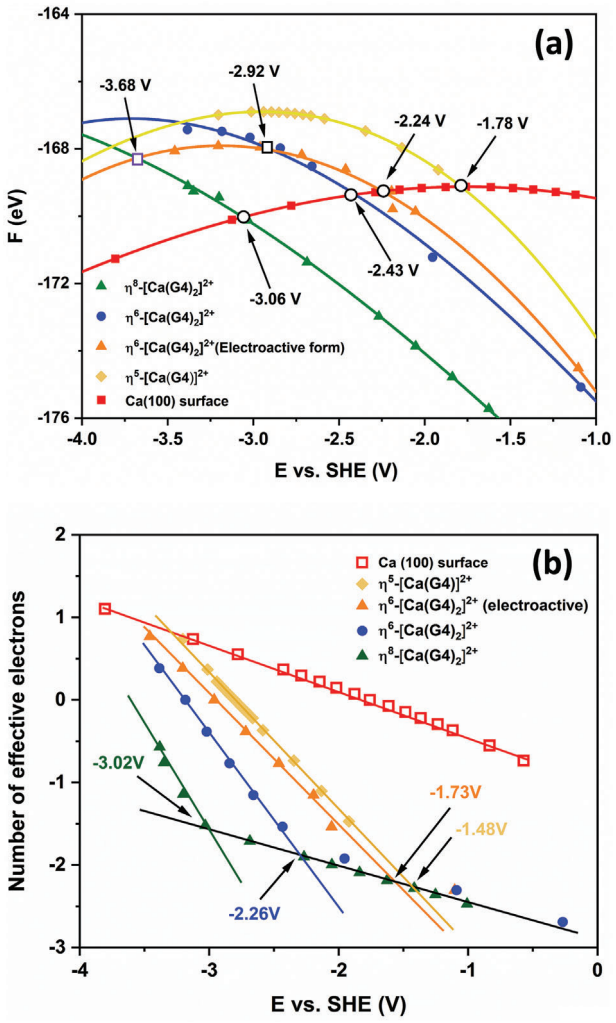

Figure 3. a) Free electrochemical energy (F) computed for the different solvated $Ca^{2+}/Ca_{surface}$ interfaces involved in the electrochemical reactions occurring at the electrode–electrolyte interface in the G4-based electrolytes. Different solvated structures with different coordination numbers for Ca^{2+} were studied, including η^5-$[Ca(G4)]^{2+}$, η^6-$[Ca(G4)_2]^{2+}$ (non-active and electroactive forms), and η^8-$[Ca(G4)_2]^{2+}$. Ca (100) surface with entropy contribution from the release of two G4 molecules from the solvation shell is used as the reference. The thermodynamic potentials at which each solvation structure is expected to undergo a reduction are marked with open circles. The potentials at which each solvation structure is converted into another form, are highlighted by open squares. b) Evolution in the number of effective electrons in the unit cell of the system as a function of the applied potential.

DFT calculations. Two glyme molecules with different lengths, for example, G1 and G4, are chosen to study the impact of metal–ligand interaction and solvent reorganization on the reactivity of solvated Ca^{2+}.

Our previous studies have shown that the strength of Ca–O interaction is independent of the length of the glyme molecules;[26,53] nevertheless, the results obtained in this new study reveal that the electroactivity of solvated Ca^{2+} in G1 and G4 is completely different (Figures 1d and 4a). In G1, the electron transfer can occur via an outer sphere pathway without the break of the primary solvation sheath. Nonetheless, the transferred electron is captured by both Ca^{2+} and G1 molecule in the solvation sphere, leading to a competition between Ca plating and solvent degradation process. Part of $[Ca(G1)_4]^{2+}$ will be converted into $Ca(G1)_3(OCH_3)_2$, which becomes electro-inactive, and a gradual capacity loss will be observed in subsequent cycles. The addition of an anion that is stable at low voltage and can act as a complexing agent, for example, Cl^- or BH_4^-, could prevent the solvent decomposition and enable long-term cycling. The case of $[Ca(G1)_4]^{2+}$ represents the situation where the electrode reaction is limited by the rate of the electron transfer process, and a faster reaction rate will occur at a shorter distance between the solvated ion and electrode surface. On the other hand, such a direct ion–electron coupling is not observed for η^8-$[Ca(G4)_2]^{2+}$. The transferred electron would reside in the proximity of η^8-$[Ca(G4)_2]^{2+}$ in the form of solvated electron. In such case, the electrode mechanism is governed by the solvent re-organization or the adsorption of the partially desolvated ion on active site on the electrode surface. This comparison reveals that the length of glyme molecules has a great impact on the mechanism of electrode reactions. At short length, the kinetics of the electrode reaction is limited by the electron transfer step while the desolvation is the limiting factor as the length of glyme molecules increases. The reason for this behavior could be due to the fact that long chain glymes possess larger strain energy, and the solvation sphere might suffer difficulties reorganizing its structure and elongate Ca–O bonds, preventing the electrons to be added to the valence shell of Ca^{2+}. Consequently, in order to enable an efficient plating, a weak M–X interaction (X is the coordinating ion in the electrolyte) or an external energy, for example, heating, is required to facilitate the desolvation process.

The key element in the reduction of η^8-$[Ca(G4)_2]^{2+}$ is the desolvation of the structure to generate the η^6-$[Ca(G4)_2]^{2+}$ species. A detailed investigation on the partially desolvated form, η^6-$[Ca(G4)_2]^{2+}$, reveals interesting structural and electrochemical properties of the system. The thermodynamically stable η^6-$[Ca(G4)_2]^{2+}$ is not electroactive at intermediate potentials; however, it will convert thermodynamically into an electroactive structure at -2.92 V_{SHE}. The conversion of inactive η^6-$[Ca(G4)_2]^{2+}$ to an electroactive form occurs through an activation process with the coupling of the Ca–O strain and the reorganization of the solvation sphere. At the equilibrium potential, the electron exchange and the conversion of η^6-$[Ca(G4)_2]^{2+}$ from non-electroactive to electroactive structure can be written as:

$$\left(\eta^6-\left[Ca\left(G_4\right)_2\right]^{2+},1e_s^-\right)+0.4e^-\leftrightarrows\eta^6-\left[Ca\left(G_4\right)_2\right]^{0.6+}_{\text{active form}} \quad (3)$$

The coupling between the two η^6-$[Ca(G4)_2]^{2+}$ redox forms can be understood in a relevant approach to Marcus theory.[54] The classical Marcus theory uses the diabatic approach, in which the reduced and oxidized species are considered independently and then the energy of two separated systems is coupled to obtain a complete view on the kinetics of the redox process. In this study, the DFT calculations corresponding to the solution of time-independent Schrödinger equation can provide an adiabatic vision of the coupling between different Ca^{2+} solvation forms within the Born–Oppenheimer limit. **Figure 5** illustrates the reaction coordinate for the conversion of non-electroactive to electroactive η^6-$[Ca(G4)_2]^{2+}$. In the adiabatic approach, the free

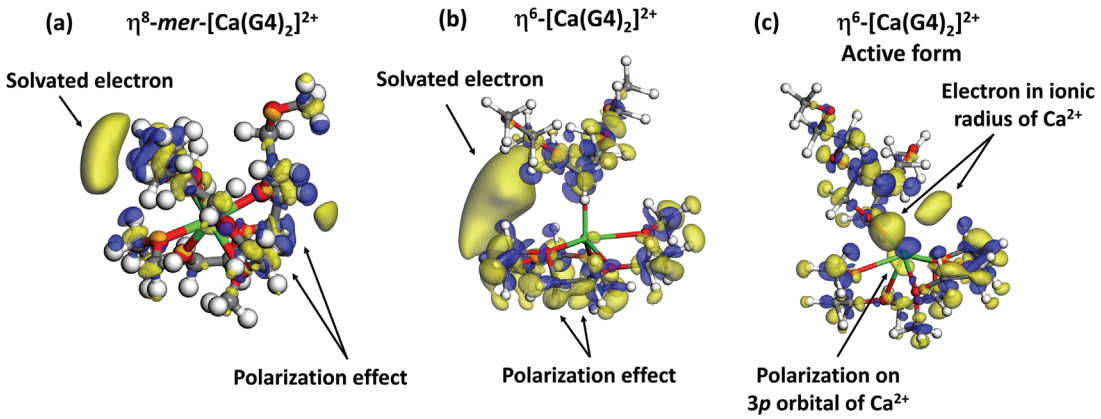

Figure 4. Fukui function calculated for a) η^8-*mer*-$[Ca(G4)_2]^{2+}$, b) η^6-$[Ca(G4)]^{2+}$, and c) active form of η^6-$[Ca(G4)]^{2+}$ at −3.35, −3.05, and −2.98 V_{SHE}, respectively. These potentials are chosen as they are below the onset required for the charge transfer to occur. The yellow and blue areas indicate electron accumulation and depletion, respectively. The majority charge accumulation is a consequence of the electron transferred from the Ca metal surface. The minority charge accumulation/depletion is a result of the polarization effect due to the presence of the transferred electron inside or outside the solvation sphere.

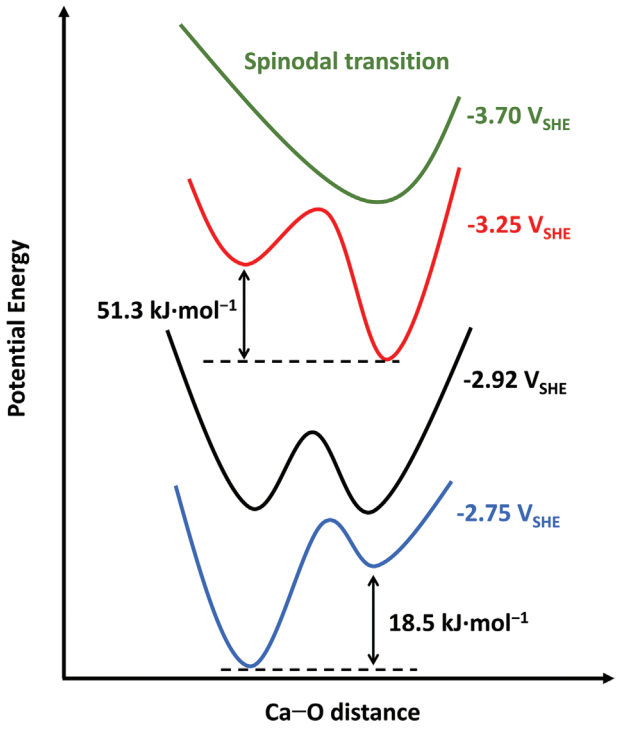

Figure 5. Schematic representation for the conversion of the non-electroactive η^6-$[Ca(G4)_2]^{2+}$ (left) to the electroactive form (right). The conversion from one solvation form to the other is coupled to the stretching of the Ca–O bonds parameter and the reorganization of the solvation sphere. The applied potential has a direct influence on the free energy of the species. At −2.92 V_{SHE}, the active and non-active forms possess the same potential energy, giving them the same probability to exist in solution.

energy of these two systems oscillates around their equilibrium Ca–O distances (defined by the x parameter), and the energy minima corresponds to $(\frac{\partial G}{\partial x})_V = 0$ and $(\frac{\partial^2 G}{\partial x^2})_V > 0$ (with V is the potential variable). The conversion between these two solvation forms is associated to a transition state and an activation energy barrier. At $E > -2.75$ V_{SHE}, the non-electroactive form, η^6-$[Ca(G4)_2]^{2+}$, is the most stable one in the solution; however, non-electroactive and electroactive η^6-$[Ca(G4)_2]^{2+}$ are isoenergetic and in equilibrium at $E = -2.92$ V_{SHE}, but a kinetic barrier still exists due to the energy required to reorganize the solvation shell, including the Ca–O elongation and angular deformation (Figure 5). As the potential goes lower, the electroactive form becomes more stable. The kinetic barrier still exists, but its absolute value decreases greatly. When the barrier energy decreases down to zero ($E < -3.70$ V_{SHE}), the energy minima of the non-electroactive η^6-$[Ca(G4)_2]^{2+}$ completely vanishes and the system evolves into the spinodal transition,[55] at which the structural vibrations allow a spontaneous conversion of inactive η^6-$[Ca(G4)_2]^{2+}$ into the active form.

The case of η^6-$[Ca(G4)_2]^{2+}$ represents an interesting "potential–vibration–electroactivity" relation, in which the applied potential controls the free energy of two different solvation species exhibiting different electroactivities and the vibrational coupling will help to convert one to the other form. Similarly, the inactive η^8-$[Ca(G4)_2]^{2+}$ can also convert to the electroactive form η^6-$[Ca(G4)_2]^{2+}$ through the de-solvation and structural reorganization at −3.68 V_{SHE} (purple open square in Figure 3a) following the redox equation.

$$\left(\eta^8 - \left[Ca\left(G_4\right)_2\right]^{2+}, 1e_s^-\right) + e^- \rightleftarrows \eta^6 - \left[Ca\left(G_4\right)_2\right]^0_{\text{active form}} \quad (4)$$

Note that the difference in the energy between the inactive η^8-$[Ca(G4)_2]^{2+}$ and the electroactive form η^6-$[Ca(G4)_2]^{2+}$ is 120 kJ mol^{-1} at −1.9 V_{SHE}, but completely vanishes at −3.68 V_{SHE}. This observation suggests that a large overpotential is required to plate calcium in this system, which is a consequence of the necessity to partially de-solvate η^8-$[Ca(G4)_2]^{2+}$ into the suitable electroactive form that only exist at a low potential.

The obtained results indicate that a partial desolvation of Ca^{2+} in G4 is required for an effective Ca plating to occur. Among all the investigated solvation forms of Ca^{2+} in G4, only η^5-$[Ca(G4)]^{2+}$

shows an interesting electrochemical behavior, in which Ca^{2+} can be reduced directly in the solvated state without the decomposition of the organic part or the formation of solvated electron. Furthermore, the reduction potential of η^5-$[Ca(G4)]^{2+}$ (-1.92 V_{SHE}) lies in the stability window of most glyme-based solvents, which can prevent the continuous solvent degradation during the battery operation. Nevertheless, η^5-$[Ca(G4)]^{2+}$ cannot exist in solutions with a surplus of G4, the cleavage of three Ca–O bonds requires an energy of -540 kJ mol^{-1} that is not achievable at room temperature. One of the possible ways to stabilize this species is by developing ionic liquids or eutectic solvents based on η^5-$[Ca(G4)]^{2+}$ and bulky anions. The concept of solvate ionic liquids is well-known for monovalent cations and has intensively developed by Watanabe's group.[56–60] When combining NaX (X^- = $TFSI^-$, $(FSO_2)_2N^-$, ClO_4^-, and PF_6^-) and G4 in the 1/1 ratio, crystalline phases [Na(G4)]X, whose melting point is rather low, can be obtained.[58] The chain length of the glyme molecule can influence the size of the solvated cation and thus the melting point of the resulted compound significantly, for instance, the melting point of $[Na(G4)][N(SO_2F)_2]$ decreases from 89.6 to 41.3 °C when G4 is replaced G5.[58] Furthermore, these solvate ionic liquids can be used as electrolytes for chargeable batteries.[61,62] This concept is not well developed for Ca^{2+}, but the theoretical results obtained in this work show that glyme-based ionic liquids would be prospective electrolytes for CIBs.

The other possibility to favorize the existence of solvated Ca^{2+} with a low coordination number is the utilization of a co-solvent. The combination of G4 with a monodentate ether ligand, such as tetrahydrofuran (THF), in the right ratio can favor the formation of $[Ca(G4)(THF)]^{2+}$, in which the Ca^{2+} possesses a coordination number of six. The low coordination number of the solvated Ca^{2+} can shift the reaction mechanism from desolvation to solvation sphere reorganization limitation. Furthermore, THF is a monodentate ligand that can be decoordinated easily, leading to the reorganization of the solvation sphere to recover the electroactive form, similar to η^5-$[Ca(G4)]^{2+}$. The same effect is also expected by a proper combination of long- and short-chain glymes, such as G4 with G1 or G2.

5. Conclusions

In this study, the electrode reaction mechanism of Ca^{2+} in glyme-based electrolyte is investigated using potential dependent DFT calculations. The potentials corresponding to the thermodynamic equilibrium values at which the electron transfer between the electrode surface and the solvated ion occur can be predicted by examining the evolution in the free electrochemical energy and charge of the system at different voltages. The same approach can also be extended to investigate the stability and reactivity of ion-pairs in solution. For the first time, the electrochemical reduction of Ca^{2+} has been shown to depend strongly on the chain length of the glyme molecules. The reaction mechanism is shifted from charge transfer to desolvation limitation as the length of glyme molecules increases. The obtained results raise a dilemma in the utilization of multidentate glyme-based systems as electrolyte for multivalent batteries. Multidentate ligands can dissolve a considerable amount of salt thanks to the strong M–O interaction; nonetheless, the electrode reaction in this case is controlled by the desolvation process. As the cation is strongly solvated, the decoordination requires a great activation energy which will induce a large overpotential. To overcome this difficulty, a mixture of glymes/ethers containing a monodentate co-solvent that possesses a weak chelating capability can be employed to favor the existence of solvated Ca^{2+} with a low coordination number and facilitate the desolvation, helping to enable the Ca plating process.

Supporting Information

Supporting Information is available from the Wiley Online Library or from the author.

Acknowledgements

This research work was funded by the European FET-Open project VIDICAT (Grant Agreement: 829145). This work was performed using HPC resources from GENCI-CINES (grant A0100910369).

Conflict of Interest

The authors declare no conflict of interest.

Data Availability Statement

The data that support the findings of this study are available in the supplementary material of this article.

Keywords

Ca-ion batteries, electroactivity, glyme-based electrolytes, potential dependent density functional theory calculations, redox reaction

Received: January 31, 2023
Revised: April 7, 2023
Published online: June 9, 2023

[1] L. Stievano, I. de Meatza, J. Bitenc, C. Cavallo, S. Brutti, M. A. Navarra, *J. Power Sources* **2021**, *482*, 228875.
[2] R. J. Gummow, G. Vamvounis, M. B. Kannan, Y. He, *Adv. Mater.* **2018**, *30*, 1801702.
[3] Y. Tian, G. Zeng, A. Rutt, T. Shi, H. Kim, J. Wang, J. Koettgen, Y. Sun, B. Ouyang, T. Chen, Z. Lun, Z. Rong, K. Persson, G. Ceder, *Chem. Rev.* **2021**, *121*, 1623.
[4] M. E. Arroyo-de Dompablo, A. Ponrouch, P. Johansson, M. R. Palacín, *Chem. Rev.* **2020**, *120*, 6331.
[5] A. Ponrouch, J. Bitenc, R. Dominko, N. Lindahl, P. Johansson, M. R. Palacin, *Energy Storage Mater.* **2019**, *20*, 253.
[6] I. D. Hosein, *ACS Energy Lett.* **2021**, *6*, 1560.
[7] T. Tojo, Y. Sugiura, R. Inada, Y. Sakurai, *Electrochim. Acta* **2016**, *207*, 22.
[8] N. Kuperman, P. Padigi, G. Goncher, D. Evans, J. Thiebes, R. Solanki, *J. Power Sources* **2017**, *342*, 414.
[9] S. Kim, L. Yin, M. H. Lee, P. Parajuli, L. Blanc, T. T. Fister, H. Park, B. J. Kwon, B. J. Ingram, P. Zapol, R. F. Klie, K. Kang, L. F. Nazar, S. H. Lapidus, J. T. Vaughey, *ACS Energy Lett.* **2020**, *5*, 3203.

[10] M. E. Purbarani, J. Hyoung, S.-T. Hong, *ACS Appl. Energy Mater.* **2021**, *4*, 7487.
[11] A. M. Melemed, D. A. Skiba, B. M. Gallant, *J. Phys. Chem. C* **2022**, *126*, 892.
[12] S. A. McClary, D. M. Long, A. Sanz-Matias, P. G. Kotula, D. Prendergast, K. L. Jungjohann, K. R. Zavadil, *ACS Energy Lett.* **2022**, *7*, 2792.
[13] N. T. Hahn, S. A. McClary, A. T. Landers, K. R. Zavadil, *J. Phys. Chem. C* **2022**, *126*, 10335.
[14] K. S. Han, N. T. Hahn, K. R. Zavadil, N. R. Jaegers, Y. Chen, J. Z. Hu, V. Murugesan, K. T. Mueller, *J. Phys. Chem. C* **2021**, *125*, 6005.
[15] D. M. Driscoll, N. K. Dandu, N. T. Hahn, T. J. Seguin, K. A. Persson, K. R. Zavadil, L. A. Curtiss, M. Balasubramanian, *J. Electrochem. Soc.* **2020**, *167*, 160512.
[16] A. M. Melemed, B. M. Gallant, *J. Electrochem. Soc.* **2020**, *167*, 140543.
[17] Z. Li, O. Fuhr, M. Fichtner, Z. Zhao-Karger, *Energy Environ. Sci.* **2019**, *12*, 3496.
[18] A. Shyamsunder, L. E. Blanc, A. Assoud, L. F. Nazar, *ACS Energy Lett.* **2019**, *4*, 2271.
[19] K. V. Nielson, T. L. Liu, *Angew. Chem., Int. Ed.* **2020**, *59*, 3368.
[20] A. Kopač Lautar, A. Hagopian, J. S. Filhol, *Phys. Chem. Chem. Phys.* **2020**, *22*, 10569.
[21] A. Kopač Lautar, J. Bitenc, T. Rejec, R. Dominko, J. S. Filhol, M. L. Doublet, *J. Am. Chem. Soc.* **2020**, *142*, 5146.
[22] A. K. Lautar, J. Bitenc, R. Dominko, J. S. Filhol, *ACS Appl. Mater. Interfaces* **2021**, *13*, 8263.
[23] P. Février, J. Gabelli, *Nat. Commun.* **2018**, *9*, 4940.
[24] J.-S. Filhol, M.-L. Doublet, *J. Phys. Chem. C* **2014**, *118*, 19023.
[25] P. Fuentealba, E. Florez, W. Tiznado, *J. Chem. Theory Comput.* **2010**, *6*, 1470.
[26] L. H. B. Nguyen, T. Picard, N. Sergent, C. Raynaud, J.-S. Filhol, M.-L. Doublet, *Phys. Chem. Chem. Phys.* **2021**, *23*, 26120.
[27] T. Binninger, D. Saraç, L. Marsh, T. Picard, M. Doublet, C. Raynaud, *J. Chem. Theory Comput.* **2023**,*19*, 1023.
[28] G. Kresse, J. Furthmüller, *Phys. Rev. B* **1996**, *54*, 11169.
[29] G. Kresse, J. Furthmüller, *Comput. Mater. Sci.* **1996**, *6*, 15.
[30] J. P. Perdew, K. Burke, M. Ernzerhof, *Phys. Rev. Lett.* **1996**, *77*, 3865.
[31] S. Grimme, J. Antony, S. Ehrlich, H. Krieg, *J. Chem. Phys.* **2010**, *132*, 154104.
[32] M. Fishman, H. L. Zhuang, K. Mathew, W. Dirschka, R. G. Hennig, *Phys. Rev. B* **2013**, *87*, 245402.
[33] K. Mathew, R. Sundararaman, K. Letchworth-Weaver, T. A. Arias, R. G. Hennig, *J. Chem. Phys.* **2014**, *140*, 084106.
[34] K. Momma, F. Izumi, *J. Appl. Crystallogr.* **2008**, *41*, 653.
[35] N. Lespes, J. S. Filhol, *J. Chem. Theory Comput.* **2015**, *11*, 3375.
[36] M. Mamatkulov, J. S. Filhol, *Phys. Chem. Chem. Phys.* **2011**, *13*, 7675.
[37] P. J. Linstrom, W. G. Mallard, *NIST Chemistry WebBook: NIST Standard Reference Database Number 69*, Vol. *20899*, National Institute of Standards and Technology, Gaithersburg, MD **2023**.
[38] R. G. Pearson, *J. Am. Chem. Soc.* **1963**, *85*, 3533.
[39] R. G. Pearson, *J. Chem. Educ.* **1968**, *45*, 581.
[40] R. G. Pearson, *J. Chem. Educ.* **1968**, *45*, 643.
[41] K. Ta, R. Zhang, M. Shin, R. T. Rooney, E. K. Neumann, A. A. Gewirth, *ACS Appl. Mater. Interfaces* **2019**, *11*, 21536.
[42] I. Shterenberg, M. Salama, H. D. Yoo, Y. Gofer, J.-B. Park, Y.-K. Sun, D. Aurbach, *J. Electrochem. Soc.* **2015**, *162*, A7118.
[43] M. Salama, I. Shterenberg, H. Gizbar, N. N. Eliaz, M. Kosa, K. Keinan-Adamsky, M. Afri, L. J. W. Shimon, H. E. Gottlieb, D. T. Major, Y. Gofer, D. Aurbach, *J. Phys. Chem. C* **2016**, *120*, 19586.
[44] J. Bitenc, M. Firm, A. Randon Vitanova, R. Dominko, *Electrochem. Commun.* **2017**, *76*, 29.
[45] C. J. Barile, R. G. Nuzzo, A. A. Gewirth, *J. Phys. Chem. C* **2015**, *119*, 13524.
[46] N. T. Hahn, J. Self, T. J. Seguin, D. M. Driscoll, M. A. Rodriguez, M. Balasubramanian, K. A. Persson, K. R. Zavadil, *J. Mater. Chem. A* **2020**, *8*, 7235.
[47] D. Alwast, J. Schnaidt, K. Hancock, G. Yetis, R. J. Behm, *ChemElectroChem* **2019**, *6*, 3009.
[48] W. A. Seddon, J. W. Fletcher, R. Catterall, F. C. Sopchyshyn, *Chem. Phys. Lett.* **1977**, *48*, 584.
[49] W. A. Seddon, J. W. Fletcher, *Radiat. Phys. Chem.* **1980**, *15*, 247.
[50] P. Quaino, E. Colombo, F. Juarez, E. Santos, G. Belletti, A. Groß, W. Schmickler, *Electrochem. Commun.* **2021**, *122*, 106876.
[51] W. Schmickler, *Chem. Phys. Lett.* **1995**, *237*, 152.
[52] E. Santos, W. Schmickler, *Chem. Rev.* **2022**, *122*, 10581.
[53] L. H. B. Nguyen, T. Picard, C. Iojoiu, F. Alloin, N. Sergent, M. L. Doublet, J. S. Filhol, *Phys. Chem. Chem. Phys.* **2022**, *24*, 21601.
[54] R. A. Marcus, *J. Chem. Phys.* **1965**, *43*, 679.
[55] K. Binder, *Rep. Prog. Phys.* **1987**, *50*, 783.
[56] T. Mandai, K. Yoshida, K. Ueno, K. Dokko, M. Watanabe, *Phys. Chem. Chem. Phys.* **2014**, *16*, 8761.
[57] S. Tsuzuki, T. Mandai, S. Suzuki, W. Shinoda, T. Nakamura, T. Morishita, K. Ueno, S. Seki, Y. Umebayashi, K. Dokko, M. Watanabe, *Phys. Chem. Chem. Phys.* **2017**, *19*, 18262.
[58] T. Mandai, R. Nozawa, S. Tsuzuki, K. Yoshida, K. Ueno, K. Dokko, M. Watanabe, *J. Phys. Chem. B* **2013**, *117*, 15072.
[59] S. Saito, H. Watanabe, Y. Hayashi, M. Matsugami, S. Tsuzuki, S. Seki, J. N. Canongia Lopes, R. Atkin, K. Ueno, K. Dokko, M. Watanabe, Y. Kameda, Y. Umebayashi, *J. Phys. Chem. Lett.* **2016**, *7*, 2832.
[60] T. Mandai, S. Tsuzuki, K. Ueno, K. Dokko, M. Watanabe, *Phys. Chem. Chem. Phys.* **2015**, *17*, 2838.
[61] S. Terada, H. Susa, S. Tsuzuki, T. Mandai, K. Ueno, K. Dokko, M. Watanabe, *J. Phys. Chem. C* **2018**, *122*, 16589.
[62] H.-M. Kwon, M. L. Thomas, R. Tatara, Y. Oda, Y. Kobayashi, A. Nakanishi, K. Ueno, K. Dokko, M. Watanabe, *ACS Appl. Mater. Interfaces* **2017**, *9*, 6014.